Revisiting Diagrams of Ice Growth Environments

Daniel M. Hueholt*

North Carolina State University, Raleigh, NC

Sandra E. Yuter†

North Carolina State University, Raleigh, NC

Matthew A. Miller

North Carolina State University, Raleigh, NC

Submitted to the Bulletin of the American Meteorological Society
11/02/2020

*Current affiliation: Department of Atmospheric Sciences, Colorado State University, Fort Collins, CO

†*Corresponding author*: Sandra E. Yuter, seyuter@ncsu.edu

ABSTRACT

Many textbooks contain outdated and erroneous information on ice growth within clouds as a function of temperature and moisture. Laboratory studies and analysis of field observations by Bailey and Hallett in a series of papers in 2002, 2004 and 2009 corrected several errors from earlier studies, but their work has not been widely disseminated. A new, simplified diagram based on Bailey and Hallett's work focuses on the five ice growth modes of edge growth, face growth, corner growth and two types of polycrystalline growth as well as a mixed category which occurs at low ice supersaturations. To aid interpretation for a variety of applications, versions of the ice growth diagram are presented in terms of relative humidity with respect to water as well as the traditional formats of relative humidity with respect to ice and vapor density excess. The myriad shapes of pristine snow crystals are the result of either a single growth type or a sequence of multiple growth types. Overlays of data from upper air soundings on the ice growth diagrams aid interpretation of expected ice properties and physical processes in winter storms.

Capsule summary. A simplified ice crystal growth diagram as a function of relative humidity with respect to water and temperature based on state of the art research.

1. Introduction

Ice crystal shapes, also known as habits, constrain cloud radiative properties and precipitation formation. When snow reaches the surface, snowflake geometries within snowpacks influence metamorphism. The expected characteristics of ice growth at given temperatures and relative humidities provide key assumptions for retrieval of ice properties using remote sensing methods. Thus, accurate depictions of ice habit as a function of air temperature and humidity are vital throughout research and operational meteorology. Ice shapes are usually visualized using an ice habit diagram, where temperature is placed on one axis, some measure of supersaturation on the other, and the habits denoted on this phase space. However, a simple Internet search for "ice habit diagram" reveals a problem–many of the available figures disagree with one another.

Unfortunately, all ice habit diagrams published prior to 2009–and many since–do not accurately describe the real atmosphere. Popular science and Internet educational sources intended for classroom use contain errors (e.g. Furukawa and Wettlaufer 2007; Libbrecht 2017, 2020; UCAR 2020). While some widely-used textbooks have accurate information (e.g. Wang 2013; Rauber and Nesbitt 2018), others contain outdated materials (e.g. Houze 2014). Errors in upper-level textbooks likely propagate to introductory meteorology texts (e.g. Hakim and Patoux 2017; Ahrens and Henson 2018). This state of confusion makes it difficult to teach accurate information about ice crystal shapes for all levels of students.

In fact, fundamental information about ice habit as a function of temperature and humidity between 0 °C and -70 °C is largely settled science. Three papers by Bailey and Hallett (2002, 2004, 2009), based on extensive field observations and laboratory experiments, make two major

changes to previous work and represent the state of the art. First, at air temperatures below -22 °C, they show ice crystals are polycrystalline (growing along multiple axes simultaneously with no strongly preferred orientation). Platelike polycrystals grow between air temperatures -22 °C and about -45 °C, and columnar polycrystals grow at temperatures less than about -45 °C, with a weak dependence on moisture near the interface of the two. Second, at low ice supersaturations and most temperatures, a mixed-growth regime is present where polycrystals, irregulars, short columns, equiaxed crystals, and plates are all possible. Bailey and Hallett (2002) describes the platelike polycrystals and explains how prior research was biased by nucleation and substrate effects. Bailey and Hallett (2004) uses a wider range of experimental conditions, and showcases the columnar polycrystals and the mixed-growth regimes. Bailey and Hallett (2009) draws on their previous results and field observations to create an updated habit diagram. Subsequent field observations have confirmed the Bailey and Hallett (2009) diagram (Bailey and Hallett 2012; Lawson et al. 2019; Kumjian et al. 2020).

Bailey and Hallett's results and habit diagram have not been widely disseminated, likely because their figures are highly complex and intended for an expert audience. This has limited the broader usage of their conclusive findings. We present a new ice growth diagram based on the science of Bailey and Hallett (2002, 2004, 2009) designed to improve science communication about ice formation, and to facilitate meteorological data visualization. We make four key changes designed to lower the cognitive load: swapping the axes, casting the diagram in terms of relative humidity with respect to water, focusing on ice growth mode rather than ice habit, and restricting the phase space to real atmospheric conditions. This new ice growth diagram is intended for use at sophomore undergraduate level and above.

Riming and aggregation are two important ice processes which fall outside the purview of the ice diagram. The ice growth diagram only describes growth from vapor deposition. Riming adds

ice mass through freezing of cloud droplets on ice crystals, not deposition, while aggregation only rearranges extant ice crystals.

2. Revisualized ice growth diagram

We introduce a version of the diagram using relative humidity with respect to water (RH_w) (Fig. 1), in addition to the traditional displays of relative humidity with respect to ice (RH_{ice}) (Fig. 2) and vapor density excess (Fig. 3). The Appendix has alternate versions of these diagrams with higher-contrast colors and information on the publicly-available software to plot the diagrams. We preserve the depictions of sharp versus more fuzzy boundaries between growth modes as described by Bailey and Hallett (2002, 2004, 2009). The presence of a transition zone from plates to polycrystalline plates between -20 °C and -22 °C is described in Bailey and Hallett (2009). There is also a lack of a sharp transition from sector plates to dendrites (Nakaya 1954; Marshall and Langleben 1954; Demange et al. 2017a). The relatively sharp transition to the mixed regime at most temperatures is documented in Bailey and Hallett (2004).

a. Decreasing temperature on the y-axis

Almost all ice habit diagrams place temperature on the x-axis and the unit of moisture (traditionally supersaturation with respect to ice or vapor density excess) on the y-axis. The earliest research into ice habit considered only the effects of temperature (Heim 1914; Weickmann 1945; aufm Kampe et al. 1951; Mason 1953). The first plots of habit simply displayed a temperature axis and indicated habits as appropriate. When moisture began to be considered, temperature remained on the abscissa and supersaturation began to be used as the ordinate (Nakaya and Sekido 1936; aufm Kampe et al. 1951; Nakaya 1954).

Swapping the axes to place decreasing temperature on the y-axis and moisture on the x-axis yields several interpretive advantages. Having temperature decrease on the y-axis mirrors the real atmosphere, where temperature generally decreases with height. This removes a layer of abstraction, simplifying interpretation in terms of the physical atmosphere. The ICAO standard atmosphere approximation maps temperature to height (ICAO 1993). We place this approximation, normalized with respect to the 0 °C level, on the y-axis on the right side of the diagram. While the real atmosphere at any given time and location often deviates from the standard atmosphere, particularly in deep convection or near air mass boundaries in winter storms, the scale on the right of the diagram provides qualitative information about where these temperatures occur in the atmosphere. Bailey and Hallett presented a version of their diagram with temperature on the y-axis and an atmospheric height approximation in a 2010 conference paper (Bailey and Hallett 2010).

b. Use of RH_w

We favor the version of the diagram using RH_w (Fig. 1) especially for undergraduate-level educational materials. RH_w is used throughout meteorology, while ice supersaturation and vapor density excess are more specialized. RH_w is also widely understood, at least intuitively, by the general public due to its use in weather forecasts. To the best of our knowledge, our diagram is the first to illustrate ice growth modes in terms of RH_w.

Figure 4 shows the RH_w version simplified to show only the physical processes that occur in different portions of the diagram. This simplification makes it an effective educational tool to explain basic concepts of ice microphysics in introductory classes. The presentation highlights the relationship between RH_w and RH_{ice} as a function of temperature. As air temperature decreases, the RH_w needed to sustain an ice cloud shrinks as well. This is in contrast to the requirement that $RH_w \geq 100\%$ for liquid phase and mixed phase clouds.

For more expert users, ice supersaturation directly connects to concepts of sublimation, which can only occur when subsaturated with respect to ice, and deposition, which can only occur at or above saturation with respect to ice. Diagrams in terms of ice supersaturation include Nakaya (1954), Kobayashi (1957), Hallett and Mason (1958), Bailey and Hallett (2009), and St-Pierre and Thériault (2015). Vapor density excess describes the density of water vapor in excess of saturation with respect to ice (units g m^{-3}). Diagrams in this format include Kobayashi (1961), Pruppacher and Klett (1997), Furukawa and Wettlaufer (2007), St-Pierre and Thériault (2015), and Libbrecht (2017). Vapor density excess is a concrete way to describe the physical quantity of water vapor, rather than expressing some percentage of saturation.

c. Simplify to growth mode rather than ice habit

One reason for the complexity of Bailey and Hallett's diagram is its focus on ice habit. Habit classifications have grown unwieldy, as the number of identifiable habits increased from the 42 in Nakaya (1954) to the 121 identified by the current standard, Kikuchi et al. (2013). No mapping exists to relate all these unique ice habits to the environmental conditions in which they form. Novel flake geometries and particle types continue to be described (Ganetis 2013; Griffin et al. 2014; Scott 2015). Further obfuscating the situation, habit terminology is used inconsistently (Bailey and Hallett 2002, 2004).

Clearly, a different approach is needed to describe the physical behavior of ice growth. While there are a huge number of habits, there are only five ice growth modes: edge, face, corner, polycrystal (platelike), and polycrystal (columnar). An ice crystal experiencing only a single growth mode results in the basic crystal geometries. Edge growth leads to hexagonal plates, face growth to columns or needles, and corner growth to sector plates or branched crystals. In the diagram we distinguish between corner growth yielding sector plates from corner growth yielding branched

including dendritic crystals as the temperature and moisture conditions for these subcategories differ. Since "dendritic" is Latin for "branched" the nomenclature can be confusing. Dendrites are the symmetric 6-branched, fern-like and stellar subcategories of 2-D branched crystals (Nakaya 1954). Other types of branched crystals are asymmetric, 3-D, or have more or less than 6 branches (Nakaya 1954; Korolev et al. 1999; Kikuchi et al. 2013; Libbrecht 2017). Platelike polycrystalline growth produces assemblages, planes, crossed plates, and spearheads, among others. Columnar polycrystalline growth results in bullet rosettes, column rosettes, basals with columns, and more. We use the designation *mixed* to describe the Bailey and Hallett (2009) category at low ice supersaturations where combinations of polycrystal, edge, and face growth modes can occur and compact faceted polycrystals, thick plates, short columns, and equiaxed columns are observed. When an ice crystal encounters multiple environments with different growth modes, a sequence of different types of growth occurs (Nakaya 1954; Hallett and Mason 1958; Bailey and Hallett 2004). Examples of sequential growth are discussed in Section 5.

d. Restrict phase space to conditions in the troposphere

By convention, the top of the troposphere is considered to be -56.5 °C (ICAO 1993). This temperature cutoff avoids the discontinuity in temperature with altitude in the ICAO standard atmosphere associated with the stratospheric temperature inversion. There are a few cases of tropospheric clouds where our diagram does not apply to because of this temperature bound, such as some convective anvil clouds (Lawson et al. 2006). The Bailey and Hallett (2009) diagram extends to -70 °C, which better captures these conditions (Korolev et al. 2000; Bailey and Hallett 2004, 2009).

Based on theoretical and observational arguments from Korolev and Mazin (2003), we cut off our diagram at a maximum *ambient* RH_w=105%. This is a departure from Bailey and Hallett

(2009), which uses an upper bound on moisture based on ventilation. Use of ambient RH is easier to grasp for students since the impact of ventilation on RH is an advanced topic in microphysics. Additionally, since there are no changes in growth mode for RH_w > 103% for any temperature even in the circumstance of RH_w > 105% one can read the growth mode off the diagram by using the value at 105%. Ambient supersaturations with respect to water above 100% can occur within updrafts when the rate of change of the equilibrium saturation vapor pressure with decreasing temperature (source) is faster than the condensation rate on activated CCN and existing drops (sink) (Rogers and Yau 1989). Supersaturations with respect to water greater than 1% are rare and ephemeral (Mason 1971; Gerber 1991). RH_w greater than 100% cannot be measured by current commercial radiosondes. Using a theoretical framework that accounted for vertical air motions, temperature, and drop sizes, Korolev and Mazin (2003) estimated a maximum ambient RH_w of 105%. We use this as our upper bound for natural *ambient* supersaturation.

Ventilation is the process by which airflow around a crystal enhances the vapor density immediately adjacent to a crystal's corners (Keller and Hallett 1982; Wang 2002; Bailey and Hallett 2004). Ventilation occurs for any nonzero airflow around a crystal and will occur for falling ice particles. Ventilation effects increase the effective RH over the ambient RH. The magnitude of the ventilation effect is difficult to quantify. Modeling studies of even simplified shapes have been restricted to qualitative descriptions of the vapor field due to computational complexity (Wang 2002). Most work has examined only simple geometries (columns and spheres), with the notable exception of Field et al. (2008) which examined aggregates. The maximum ventilation line in Bailey and Hallett (2009) is approximated by twice the ice supersaturation at RH_w=100% for each temperature (note that this is distinct from both 200% RH_w and 200% RH_{ice}). The maximum ventilation value is intended to represent the upper bound on the conditions experienced *at* a growing crystal (Bailey and Hallett 2004). Drawbacks to using the maximum estimated ventilation in the diagram as the

upper bound on moisture are that it overconstrains supersaturations near 0 °C and underconstrains supersaturations at low temperatures near -40 °C.

An air parcel within an updraft can experience a pulse of positive buoyancy from the release of latent heat of freezing drops. Updrafts are weaker in the upper troposphere than at lower altitudes and ambient upper-tropospheric relative humidities rarely reach 80% RH_w (Lang et al. 2020). Ambient supersaturations of RH_w> 105% are possible within a laboratory, but we are not aware of any field observations or theoretical arguments that show these conditions to be possible in the real atmosphere (Hallett and Mason 1958; Bailey and Hallett 2004).

Laboratory work has demonstrated unique ice growth behavior at extreme supersaturations in certain temperature ranges. High-temperature (0 °C to -4 °C) dendritic plates and fishbone dendrites require RH_w values of up to 200% (Hallett and Mason 1958; Libbrecht 2009). But, as these conditions are never achieved in Earth's atmosphere, these habits cannot occur in natural clouds and storms. The existence of these extreme crystals is interesting, but we believe it is necessary to only display real atmospheric conditions in our diagram intended for education and atmospheric research.

3. Ice growth modes from atmospheric profiles

Profiles of temperature and RH_w from observations or models can be plotted on the diagram to reveal the ice growth modes at different altitudes. Potentially, this type of analysis can be used to recontextualize the entire global soundings data set, which can now be harvested for information about which growth modes are most frequent as a function of geography. Overlaying atmospheric profiles from weather and climate numerical model output on the ice growth diagram provides a means of interpreting the model's implied ice growth modes as well as evaluating predicted growth

modes compared to observations. Analysis in terms of ice growth modes can constrain ice shapes which are important for cloud radiative properties.

When interpreting observed radiosonde data overlaid on the ice growth diagrams, several items need to be kept in mind. Commercial radiosondes cannot measure supersaturations with respect to water. In particular, this means these data cannot be used to identify precisely where corner branched growth occurs. Qualitatively, we infer higher probabilities for branched and dendritic growth by ventilation for the subset of points with RH_w above 95% in the proper temperature range. The radiosonde characterizes the environment, not any individual crystal. Precipitation-sized ice experiences multiple growth conditions as it falls (sediments), and may experience other local effects, especially ventilation. A point on an ice growth profile describes the mode of ice growth occurring in that portion of the profile at a particular time. Snowflake habits at the surface are constrained by the actual conditions for ice growth aloft for a particular storm or season.

We contrast winter season radiosonde data sets from December 2014 through February 2015 from a mid-latitude maritime, a polar, and a continental site in the Northern Hemisphere in Figure 5. All soundings during the period are used in these plots whether a winter storm was present or not. We chose the 2014-2015 season to obtain an ENSO-neutral time period. These three examples illustrate the prevalence of conditions for mixed and polycrystal growth modes within the colder cloud tops at all three locations.

The example mid-latitude maritime environment is from the National Weather Service's sounding site in Upton, New York (Fig. 5a). Most of the ice growth occurs at relatively warm temperatures. The points are clustered most densely between 0 °C and -10 °C. In comparison, there are few points near water saturation in the -12 °C to -18 °C range. It is important to distinguish between conditions conducive to ice nucleation as compared to those necessary for ice growth. Once an initial ice embryo forms it can grow by vapor deposition if $RH_{ice} \geq 100\%$. In contrast to common

inorganic ice nuclei, biological nuclei can activate at temperatures higher than -10 °C (Schnell and Vali 1976; Vali et al. 1976; Christner et al. 2008; J. Murray et al. 2012; Michaud et al. 2014; Kanji et al. 2017). Given the prevalence of cloud conditions at temperatures > -10 °C, these seasonal data suggest biological nuclei may be important contributors to ice formation along the U.S. eastern seaboard.

We use the Department of Energy Atmospheric Radiation Measurement research site in Utqiagvik, Alaska above the Arctic Circle and along the coast of the Beaufort Sea as our polar environment example in Figure 5b (DOE-ARM 2020). As expected, the set of profiles are colder than in the mid-latitudes. Ambient conditions are are dominated by edge growth, the mixed regime, platelike polycrystals, and columnar polycrystals.

The example midlatitude continental location is the National Weather Service's radiosonde site at Denver, Colorado (Figure 5c). As an interior continental site, Denver's seasonal profile is far drier than either Upton, NY or Utqiagvik, AK. There are no points near water saturation in the -12 °C to -18 °C range. The overall sparseness of points within the ice growth regions of the diagram indicates background ambient conditions at Denver are rarely sufficient to maintain ice growth. In addition to synoptic-scale vertical motions along air mass boundaries, mesoscale upslope flows and vertical motions from waves such as those forced by topography are likely critical to locally enhance supersaturations within clouds in this region.

4. Rapid ice growth conditions encompass more than dendrites

The higher the vapor density excess over ice saturation, the faster the vapor deposition growth rate for a given moisture content of the air (water vapor mixing ratio) (Rogers and Yau 1989; Houze 2014; Harrison et al. 2016). The peak vapor density excess occurs at -12 °C for RH_w=100%, at -10 °C for RH_w=102.5%, and at -8 °C for RH_w=105% (Fig. 3). The maximum vapor density

excess at RH_w=105% and -8 °C is near the boundary between corner growth and face growth. At RH_w=102.5%, higher values of vapor density excess occur for face growth (column-like) and corner growth (sector plates) than for corner growth (branched, dendrites). For similar supersaturations with respect to water, the vapor density excesses in the 0 °C to -10 °C range can approach those in the -12 °C to -18 °C range.

The temperature range -12 °C to -18 °C is sometimes labeled the "dendritic growth zone" and is often emphasized as a region of rapid ice growth (Kumjian et al. 2014; Rauber et al. 2017; Demange et al. 2017b; NWS 2017). Since dendritic growth requires both temperatures between -12 °C to -18 °C and RH_w > 101.5%, it is mistaken to infer this type of growth based only on temperature conditions. Further, dendrites are an unrepresentative subset of the possible varieties of corner branched crystals (Korolev et al. 1999; Bailey and Hallett 2009; Libbrecht 2017). Fundamentally, there is no set of atmospheric conditions that guarantees symmetrical, fernlike dendrites will occur exclusively. Focusing on dendritic growth is physically imprecise and misleading. We suggest retiring the term "dendritic growth zone".

Misinterpretation and overemphasis of "dendritic growth zone" is in part responsible for the mistaken impressions that other ice growth modes cannot gain mass rapidly and that snow primarily consists of pristine dendrites. Instead, we prefer the term *rapid growth zone* to describe situations where near water saturation is expected, vapor density excess is > 0.2 g m^{-3}, and air temperatures are between -7 °C and -19 °C. *Rapid growth zone* more fully describes the diverse growth modes occurring in these conditions.

5. The importance of sequential growth

Within a cloud at temperatures less than 0 °C, ambient conditions are typically such that $RH_{ice} \geq 100\%$ but RH_w is usually not ≥ 100%. An ice crystal can undergo a sequence of

distinct growth modes as it falls through different temperature and moisture conditions. Hence, the resulting ice crystal habit can be described by this sequence of growth modes. These sequences can be identified using high-resolution particle imagers such as the SPEC Inc. Cloud Particle Imager (CPI), Particle Flux Analytics Multi-Angle Snowflake Camera (MASC), and the Institute for Meteorology and Climate Research's Particle Habit Imaging and Scattering Probe (PHIPS) (Lawson et al. 2001; Garrett et al. 2012; Abdelmonem et al. 2016). We describe three well-known habits that can be described by their growth mode sequences. For habit terminology, we use the classification nomenclature of Kikuchi et al. (2013). The example ice crystal images are from the CPI mounted on the NASA P-3 aircraft during the Investigation of Microphysics and Precipitation for Atlantic Coast-Threatening Snowstorms (IMPACTS) field campaign in 2020 (McMurdie et al. 2019; NASA 2020). The images were collected within a 4 minute span of time when the NASA P-3 was near the border of Massachusetts and Vermont as the aircraft climbed from 4.2 km to 4.9 km altitude. The different crystal types observed within close proximity to each other illustrate that ice particles often leave the conditions where they were formed and mix through vertical air motions, advection, and sedimentation.

An example of a "plate with branches" or "P4e" habit is shown in Figure 6. We identify the sequence yielding this crystal as edge growth (forming the central irregular hexagonal plate) followed by corner growth (yielding the 6 fernlike branches on the corners). Ventilation is likely responsible for this sequence. Corner growth requires suitable temperatures and supersaturation with respect to water, which is difficult to maintain in a mixed or ice phase cloud (Mason 1971; Korolev and Mazin 2003). Edge growth requires suitable temperatures and supersaturation with respect to ice and is easier to achieve. Once a crystal grows by edge growth (yielding a hexagonal plate) to a large enough size to fall, ventilation can increase the supersaturation adjacent to the plate's corners such that corner growth begins. Qualitatively, reviewing large numbers of CPI

images indicates that most branched crystals including dendrites have an inner core of a hexagonal plate. The implication is that edge growth followed by corner growth is a common pathway to produce branched crystals. This image was obtained at 22:08:38 UTC on January 25, 2020 at an altitude of 4.86 km. The in situ environmental conditions were RH_{ice} of 101.5%, RH_w of 88.4%, and an air temperature of -13.9 °C. These values indicate that the crystal had left the conditions necessary for corner growth and was in mixed growth conditions.

An example of the habit informally known as "capped column" (Libbrecht 2017) is shown in Figure 7. Kikuchi et al. (2013) does not distinguish columns capped with sector plates from columns capped with dendrites in their category "column with dendrites" or "CP1b" habit (their Fig. 1-CP1b). The sequence producing this crystal is face growth (forming the central column) followed by corner growth (yielding the sector plates on the end). Vertical motion, likely accompanied by ventilation, is a likely physical pathway for this sequence. The crystal must both be cooled below -8 °C and moistened above water saturation to switch from face to corner growth. An enhancement of supersaturation alone, as caused by ventilation, cannot cause this growth sequence. This image was captured at 22:05:45 UTC on January 25, 2020 at an altitude of 4.21 km. In situ environmental conditions corresponding to the image are RH_{ice} of 102.2%, RH_w of 93.0%, and an air temperature of -9.5 °C indicating mixed growth conditions.

Bailey and Hallett (2009) describe mixed rosettes (their Fig. 7) in terms of a sequence of growth modes, specifically, polycrystal (columnar) growth followed by polycrystal (platelike) growth. This sequence often likely occurs through sedimentation–a crystal forming in the columnar polycrystal temperatures falls into the warmer platelike polycrystal regime. Because of their formation through sedimentation, these crystal shapes may be frequently seen at thermodynamic conditions far from their cold formation temperatures. Figure 8 shows an example of a mixed rosette or "P7a" habit. This image was taken at 22:08:52 UTC at January 25, 2020 at an altitude of 4.86 km. The aircraft

was outside of cloud at this time since RH_{ice} was 90.7%, RH_w was 79.5%, and environmental temperature was -13.3 °C.

6. Summary and concluding remarks

General understanding of ice microphysics has been hindered by slow adoption of crucial corrections (Bailey and Hallett 2002, 2004, 2009) to previous work in materials targeted for student use. We revisualize the current state of the art ice habit diagram in Bailey and Hallett (2009) by simplifying the dozens of ice habits to five ice growth modes and recasting the diagram in terms of RH_w with the goals of improving clarity and ease of use. Use of RH_w puts ice microphysics into a more accessible framework for students than RH_{ice} or vapor density excess. The decreasing RH_w needed for ice saturation and cloud formation as a function of decreasing air temperature is readily apparent. The important distinction that both of the two types of corner growth (sector plates or branched and dendrites) requires supersaturation with respect to water whereas all the other growth modes do not is shown clearly.

In addition to the educational applications, we see several pathways to apply the ice growth diagram in research. We think it is possible that many, if not all, observed pristine ice habits are reducible to their component growth mode sequences. Joint analysis of high resolution ice particle images and thermodynamic profiles in the context of the ice growth diagram has the potential to yield a classification system for ice crystals based on growth modes. Plotting atmospheric profiles from observed radiosonde data and weather and climate model output on the ice growth diagram can provide insight on where and why differences between model physics and the real atmosphere occur. Analysis of the decades-long radiosonde archive in the context of ice growth diagram may yield insights into impacts of the changing climate on ice cloud properties.

Data availability statement. National Weather Service radiosonde data from Upton, NY and Denver, CO can be obtained from the Integrated Global Radiosonde Archive, Version 2 described in Durre et al. (2006).

Department of Energy Atmospheric Radiation Measurement radiosonde data from the North Slope Alaska Central Facility site at Utqiagvik, AK are accessible from doi.org/10.5439/1021460.

Cloud Particle Imager data from the NASA Investigation of Microphysics and Precipitation for Atlantic Coast-Threatening Snowstorms field campaign can be accessed from doi.org/10.5067/IMPACTS/PROBES/DATA101.

Acknowledgments. The development and refinement of the ice growth diagrams benefited from discussions with David Kingsmill. Aaron Bansemer and David Delene provided the NASA IMPACTS CPI data and Ryan Bennett supplied the NASA P-3 flight-level data. Special thanks to Laura Tomkins, Levi Lovell, and Ronak Patel for their input on visualization options. This work was supported by the National Science Foundation (AGS-1347491 and AGS-1905736), the National Aeronautics and Space Administration (80NSSC19K0354), and the North Carolina State University Honors Program (Hueholt).

APPENDIX

Software for plotting ice growth diagrams

Our software to plot the ice growth diagrams in formats with muted colors and labels on the diagram (Figs. 1, 2, 3) and with brighter colors and a key at the bottom of the diagram (Appendix figures) is on the Open Science Foundation website. The MATLAB code and documentation can be accessed at https://osf.io/g9vzj/

MATLAB code to plot data from the Integrated Global Radiosonde Archive on the ice growth diagrams is included in the package. The RH_w and RH_{ice} versions are better suited than the vapor density excess version for overlaying radiosonde data. At low temperatures, the atmosphere reaches saturation at small vapor density excess. Thus, the vapor density excess diagram narrows drastically at low temperatures, particularly below approximately -30 °C, and data points are jumbled on top of each other.

The package also includes functions to convert between the various moisture variables. This is particularly useful for conversions to and from vapor density excess, which can be unintuitive.

References

Abdelmonem, A., E. Järvinen, D. Duft, E. Hirst, S. Vogt, T. Leisner, and M. Schnaiter, 2016: PHIPS–HALO: the airborne Particle Habit Imaging and Polar Scattering probe – Part 1: Design and operation. *Atmospheric Measurement Techniques*, **9 (7)**, 3131–3144, doi:https://doi.org/10.5194/amt-9-3131-2016.

Ahrens, C. D., and R. Henson, 2018: *Meteorology Today: An Introduction to Weather, Climate and the Environment*. 12th ed., Cengage Learning, Boston, MA.

aufm Kampe, H. J., H. K. Weickmann, and J. J. Kelly, 1951: The influence of temperature on the shape of ice crystals growing at water saturation. *J. Meteor.*, **8 (3)**, 168–174, doi:10.1175/1520-0469(1951)008<0168:TIOTOT>2.0.CO;2.

Bailey, M., and J. Hallett, 2002: Nucleation effects on the habit of vapour grown ice crystals from 18 to 42°C. *Q.J.R. Meteorol. Soc.*, **128 (583)**, 1461–1483, doi:10.1002/qj.200212858304.

Bailey, M., and J. Hallett, 2004: Growth Rates and Habits of Ice Crystals between 20° and 70°C. *J. Atmos. Sci.*, **61 (5)**, 514–544, doi:10.1175/1520-0469(2004)061<0514:GRAHOI>2.0.CO;2.

Bailey, M., and J. Hallett, 2010: Laboratory Measured Ice Crystal Capacitances & Mass Dimensional Relations, Portland, OR. 16.

Bailey, M., and J. Hallett, 2012: Ice Crystal Linear Growth Rates from 20° to 70°C: Confirmation from Wave Cloud Studies. *J. Atmos. Sci.*, **69 (1)**, 390–402, doi:10.1175/JAS-D-11-035.1.

Bailey, M. P., and J. Hallett, 2009: A Comprehensive Habit Diagram for Atmospheric Ice Crystals: Confirmation from the Laboratory, AIRS II, and Other Field Studies. *J. Atmos. Sci.*, **66 (9)**, 2888–2899, doi:10.1175/2009JAS2883.1.

Christner, B. C., C. E. Morris, C. M. Foreman, R. Cai, and D. C. Sands, 2008: Ubiquity of biological ice nucleators in snowfall. *Science*, **319 (5867)**, 1214, doi:10.1126/science.1149757.

Demange, G., H. Zapolsky, R. Patte, and M. Brunel, 2017a: Growth kinetics and morphology of snowflakes in supersaturated atmosphere using a three-dimensional phase-field model. *Phys. Rev. E*, **96 (2)**, 022 803, doi:10.1103/PhysRevE.96.022803.

Demange, G., H. Zapolsky, R. Patte, and M. Brunel, 2017b: A phase field model for snow crystal growth in three dimensions. *npj Comput Mater*, **3 (1)**, 15, doi:10.1038/s41524-017-0015-1.

DOE-ARM, 2020: Balloon-borne sounding system (sondewnpn). doi:10.5439/1021460.

Durre, I., R. S. Vose, and D. B. Wuertz, 2006: Overview of the Integrated Global Radiosonde Archive. *J. Climate*, **19 (1)**, 53–68, doi:10.1175/JCLI3594.1.

Field, P. R., J. Heymsfield, A. Bansemer, and C. H. Twohy, 2008: Determination of the Combined Ventilation Factor and Capacitance for Ice Crystal Aggregates from Airborne Observations in a Tropical Anvil Cloud. *J. Atmos. Sci.*, **65 (2)**, 376–391, doi:10.1175/2007JAS2391.1.

Furukawa, Y., and J. S. Wettlaufer, 2007: Snow and ice crystals. *Physics Today*, **60 (12)**, 70–71, doi:10.1063/1.2825081.

Ganetis, S. A., 2013: Evolution of an Intense Mesoscale Snowband During the 8–9 February 2013 Northeast U.S. Blizzard. URL https://ams.confex.com/ams/15MESO/webprogram/Paper228054.html.

Garrett, T. J., C. Fallgatter, K. Shkurko, and D. Howlett, 2012: Fall speed measurement and high-resolution multi-angle photography of hydrometeors in free fall. *Atmos. Meas. Tech.*, **5 (11)**, 2625–2633, doi:10.5194/amt-5-2625-2012.

Gerber, H., 1991: Supersaturation and Droplet Spectral Evolution in Fog. *J. Atmos. Sci.*, **48 (24)**, 2569–2588, doi:10.1175/1520-0469(1991)048<2569:SADSEI>2.0.CO;2.

Griffin, E. M., T. J. Schuur, A. V. Ryzhkov, H. D. Reeves, and J. C. Picca, 2014: A Polarimetric and Microphysical Investigation of the Northeast Blizzard of 8–9 February 2013. *Wea. Forecasting*, **29 (6)**, 1271–1294, doi:10.1175/WAF-D-14-00056.1.

Hakim, G. J., and J. Patoux, 2017: *Weather A Concise Introduction*. Academic Press.

Hallett, J., and B. J. Mason, 1958: The influence of temperature and supersaturation on the habit of ice crystals grown from the vapour. *Proc. R. Soc. Lond. A*, **247 (1251)**, 440–453, doi:10.1098/rspa.1958.0199.

Harrison, A., A. M. Moyle, M. Hanson, and J. Y. Harrington, 2016: Levitation Diffusion Chamber Measurements of the Mass Growth of Small Ice Crystals from Vapor. *J. Atmos. Sci.*, **73 (7)**, 2743–2758, doi:10.1175/JAS-D-15-0234.1.

Heim, F., 1914: Diamantstaub und Schneekristalle in der Antarktis (Wedellsee). *Meteorologische Zeitschrift*, **31**, 232–235.

Houze, R. A., Jr., 2014: *Cloud dynamics*. Amsterdam ; New York : Academic Press is an imprint of Elsevier, [2014].

ICAO, 1993: *Manual of the ICAO Standard Atmosphere: extended to 80 kilometres (262 500 feet)*, Vol. 7488. International Civil Aviation Organization.

J. Murray, B., D. O'Sullivan, J. D. Atkinson, and M. E. Webb, 2012: Ice nucleation by particles immersed in supercooled cloud droplets. *Chemical Society Reviews*, **41 (19)**, 6519–6554, doi:10.1039/C2CS35200A.

Kanji, Z. A., L. A. Ladino, H. Wex, Y. Boose, M. Burkert-Kohn, D. J. Cziczo, and M. Krämer, 2017: Overview of Ice Nucleating Particles. *Meteor. Monogr.*, **58**, 1.1–1.33, doi:10.1175/AMSMONOGRAPHS-D-16-0006.1.

Keller, V., and J. Hallett, 1982: Influence of air velocity on the habit of ice crystal growth from the vapor. *Journal of Crystal Growth*, **60 (1)**, 91–106, doi:10.1016/0022-0248(82)90176-2.

Kikuchi, K., T. Kameda, K. Higuchi, and A. Yamashita, 2013: A global classification of snow crystals, ice crystals, and solid precipitation based on observations from middle latitudes to polar regions. *Atmospheric Research*, **132-133**, 460–472, doi:10.1016/j.atmosres.2013.06.006.

Kobayashi, T., 1957: Experimental Researches en the Snow Crystal Habit and Growth by Means of a Diffusion Cloud Chamber. *Journal of the Meteorological Society of Japan*, **35A (0)**, 38–47, doi:10.2151/jmsj1923.35A.0_38.

Kobayashi, T., 1961: The growth of snow crystals at low supersaturations. *Philosophical Magazine*, **6 (71)**, 1363–1370, doi:10.1080/14786436108241231.

Korolev, A., G. A. Isaac, and J. Hallett, 2000: Ice particle habits in stratiform clouds. *Quarterly Journal of the Royal Meteorological Society*, **126 (569)**, 2873–2902, doi:10.1002/qj.49712656913.

Korolev, A. V., G. A. Isaac, and J. Hallett, 1999: Ice particle habits in Arctic clouds. *Geophysical Research Letters*, **26 (9)**, 1299–1302, doi:10.1029/1999GL900232.

Korolev, A. V., and I. P. Mazin, 2003: Supersaturation of Water Vapor in Clouds. *J. Atmos. Sci.*, **60 (24)**, 2957–2974, doi:10.1175/1520-0469(2003)060<2957:SOWVIC>2.0.CO;2.

Kumjian, M. R., K. A. Bowley, P. M. Markowski, K. Lombardo, Z. J. Lebo, and P. Kollias, 2020: Snowflake Selfies: A Low-Cost, High-Impact Approach toward Student Engagement in

Scientific Research (with Their Smartphones). *Bull. Amer. Meteor. Soc.*, **101 (6)**, E917–E935, doi:10.1175/BAMS-D-19-0096.1.

Kumjian, M. R., S. A. Rutledge, R. M. Rasmussen, P. C. Kennedy, and M. Dixon, 2014: High-Resolution Polarimetric Radar Observations of Snow-Generating Cells. *J. Appl. Meteor. Climatol.*, **53 (6)**, 1636–1658, doi:10.1175/JAMC-D-13-0312.1.

Lang, T., S. A. Buehler, M. Burgdorf, I. Hans, and V. O. John, 2020: A new climate data record of upper-tropospheric humidity from microwave observations. *Scientific Data*, **7 (1)**, 218, doi:10.1038/s41597-020-0560-1.

Lawson, R. P., B. Baker, B. Pilson, and Q. Mo, 2006: In Situ Observations of the Microphysical Properties of Wave, Cirrus, and Anvil Clouds. Part II: Cirrus Clouds. *J. Atmos. Sci.*, **63 (12)**, 3186–3203, doi:10.1175/JAS3803.1.

Lawson, R. P., B. A. Baker, C. G. Schmitt, and T. L. Jensen, 2001: An overview of microphysical properties of Arctic clouds observed in May and July 1998 during FIRE ACE. *Journal of Geophysical Research: Atmospheres*, **106 (D14)**, 14 989–15 014, doi:10.1029/2000JD900789.

Lawson, R. P., and Coauthors, 2019: A Review of Ice Particle Shapes in Cirrus formed In Situ and in Anvils. *Journal of Geophysical Research: Atmospheres*, **124 (17-18)**, 10 049–10 090, doi:10.1029/2018JD030122.

Libbrecht, K. G., 2009: Identification of a Novel "Fishbone" Structure in the Dendritic Growth of Columnar Ice Crystals. *arXiv:0912.2522 [cond-mat]*.

Libbrecht, K. G., 2017: Physical Dynamics of Ice Crystal Growth. *Annu. Rev. Mater. Res.*, **47 (1)**, 271–295, doi:10.1146/annurev-matsci-070616-124135.

Libbrecht, K. G., 2020: Guide to Snowflakes - SnowCrystals.com. URL http://www.snowcrystals.com/morphology/morphology.html.

Marshall, J., and M. Langleben, 1954: A Theory of Snow-Crystal Habit and Growth. *Journal of Meteorology*, **11**, 104–120.

Mason, B. J., 1953: The growth of ice crystals in a supercooled water cloud. *Quarterly Journal of the Royal Meteorological Society*, **79 (339)**, 104–111, doi:10.1002/qj.49707933909.

Mason, B. J. B. J., 1971: *The physics of clouds*. 2nd ed., Oxford monographs on meteorology., Clarendon Press, Oxford.

McMurdie, L. A., G. M. Heymsfield, S. A. Braun, and J. E. Yorks, 2019: IMPACTS: A NASA Earth-Venture Suborbital-3 Airborne Field Campaign to Investigate U.S. East Coast Snowstorms. AMS, URL https://ams.confex.com/ams/18MESO/meetingapp.cgi/Paper/361168.

Michaud, A. B., J. E. Dore, D. Leslie, W. B. Lyons, D. C. Sands, and J. C. Priscu, 2014: Biological ice nucleation initiates hailstone formation. *Journal of Geophysical Research: Atmospheres*, **119 (21)**, 12,186–12,197, doi:10.1002/2014JD022004.

Nakaya, U., and Y. Sekido, 1936: General classification of snow crystals and their frequency of occurrence. = *Journal of the Faculty of Science, Hokkaido Imperial University. Ser. 2, Physics*, **1 (9)**, 243–264.

Nakaya, U., 1900-1962, 1954: *Snow crystals, natural and artificial.* Cambridge : Harvard University Press, 1954.

NASA, 2020: IMPACTS. URL https://espo.nasa.gov/impacts/content/IMPACTS.

NWS, A., 2017: Winter Precipitation Types. URL https://www.weather.gov/ama/winterpreciptypes, publisher: NOAA's National Weather Service.

Pruppacher, H. R., 1930, and J. D. Klett, 1940, 1997: *Microphysics of clouds and precipitation*. Dordrecht ; Boston : Kluwer Academic Publishers, [1997].

Rauber, R. M., S. M. Ellis, J. Vivekanandan, J. Stith, W.-C. Lee, G. M. McFarquhar, B. F. Jewett, and A. Janiszeski, 2017: Finescale Structure of a Snowstorm over the Northeastern United States: A First Look at High-Resolution HIAPER Cloud Radar Observations. *Bull. Amer. Meteor. Soc.*, **98 (2)**, 253–269, doi:10.1175/BAMS-D-15-00180.1.

Rauber, R. M., and S. W. Nesbitt, 2018: *Radar meteorology : a first course*. Hoboken, NJ : John Wiley & Sons, 2018., Hoboken, NJ.

Rogers, R. R., and M. K. Yau, 1989: *A Short Course in Cloud Physics*, International Series in Natural Philosophy, Vol. 113. 3rd ed., Pergamon Press.

Schnell, R. C., and G. Vali, 1976: Biogenic Ice Nuclei: Part I. Terrestrial and Marine Sources. *J. Atmos. Sci.*, **33 (8)**, 1554–1564, doi:10.1175/1520-0469(1976)033<1554:BINPIT>2.0.CO;2.

Scott, E., 2015: Freshly Falling Snow: Identifying New Snowflake Geometries From Photographs. Online, URL https://education.agu.org/files/2015/11/scott.pdf.

St-Pierre, M., and J. M. Thériault, 2015: Clarification of the Water Saturation Represented on Ice Crystal Growth Diagrams. *J. Atmos. Sci.*, **72 (7)**, 2608–2611, doi:10.1175/JAS-D-14-0357.1.

UCAR, 2020: *Snowpack and its Assessment: Snow Microphysics*. 2009th ed., Comet Meted, The University Corporation for Atmospheric Research, Boulder, CO.

Vali, G., M. Christensen, R. W. Fresh, E. L. Galyan, L. R. Maki, and R. C. Schnell, 1976: Biogenic Ice Nuclei. Part II: Bacterial Sources. *J. Atmos. Sci.*, **33 (8)**, 1565–1570, doi:10.1175/1520-0469(1976)033<1565:BINPIB>2.0.CO;2.

Wang, P. K., 2002: *Ice microdynamics*. Academic Press, San Diego, Calif.

Wang, P. K., 2013: *Physics and dynamics of clouds and precipitation*. Cambridge : Cambridge University Press, 2013.

Weickmann, H., 1945: Formen und bildung atmosphaerischer eiskristalle. *Beiträge zur Physik der Atmosphäre*, **28**, 12–52.

LIST OF FIGURES

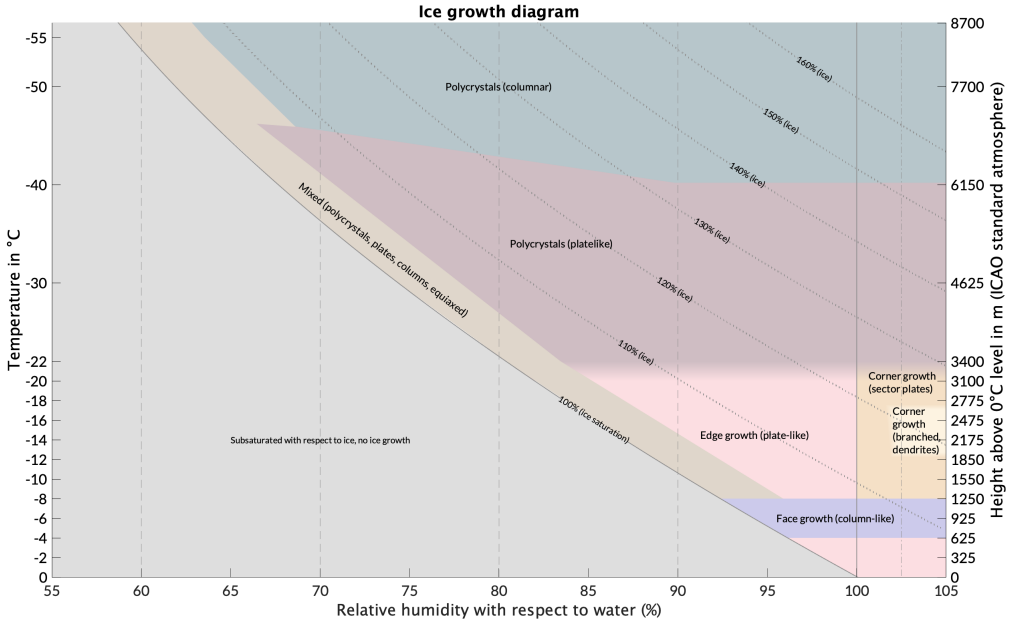

FIG. 1: Ice growth diagram in terms of relative humidity with respect to water (RH_W).

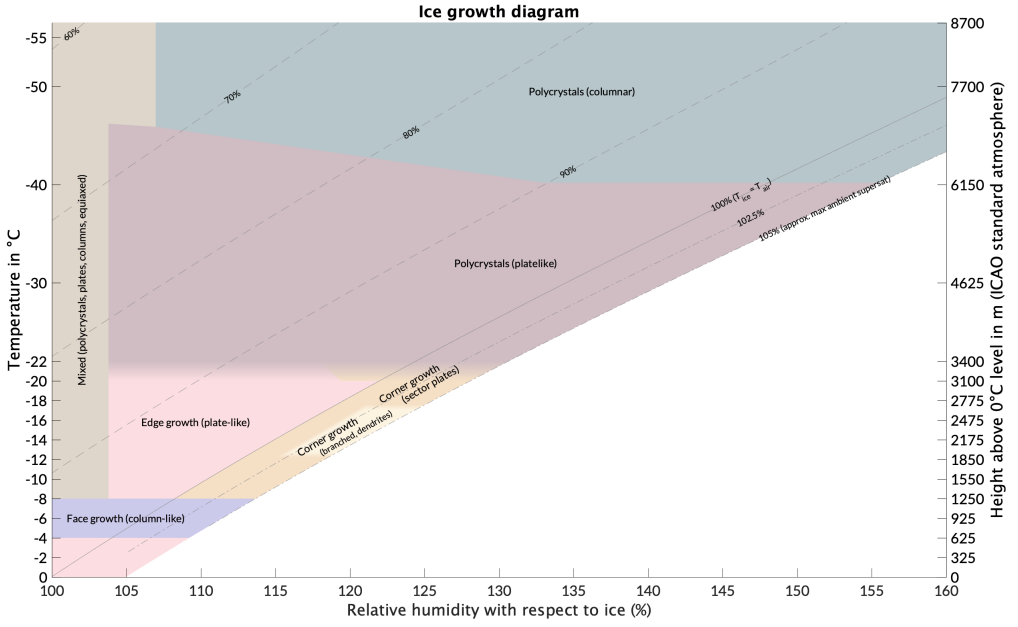

FIG. 2: Ice growth diagram in terms of relative humidity with respect to ice (RH_{ice})

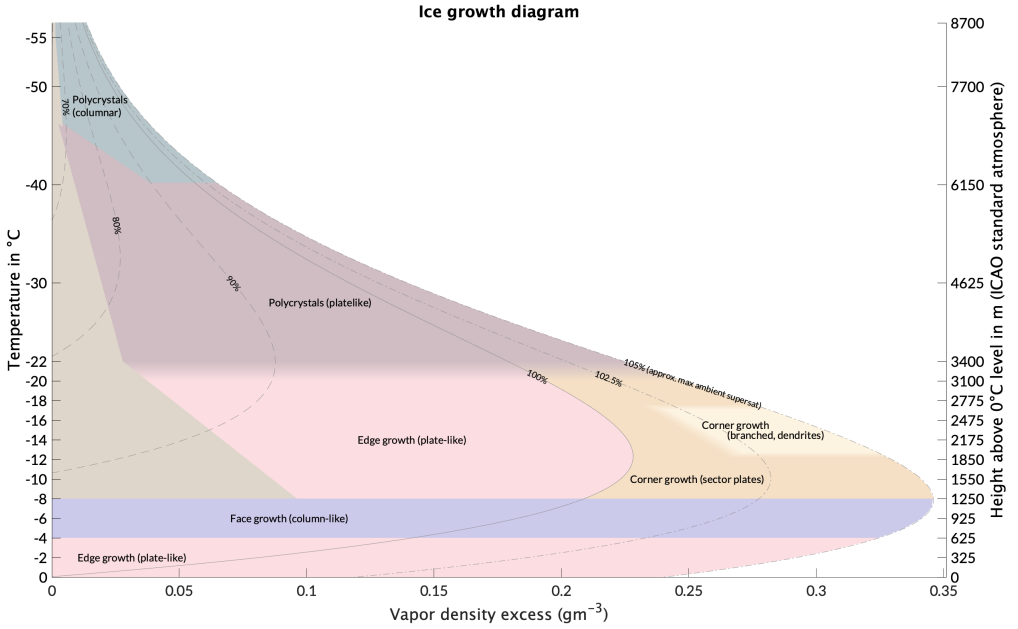

FIG. 3: Ice growth diagram in terms of vapor density excess over ice saturation.

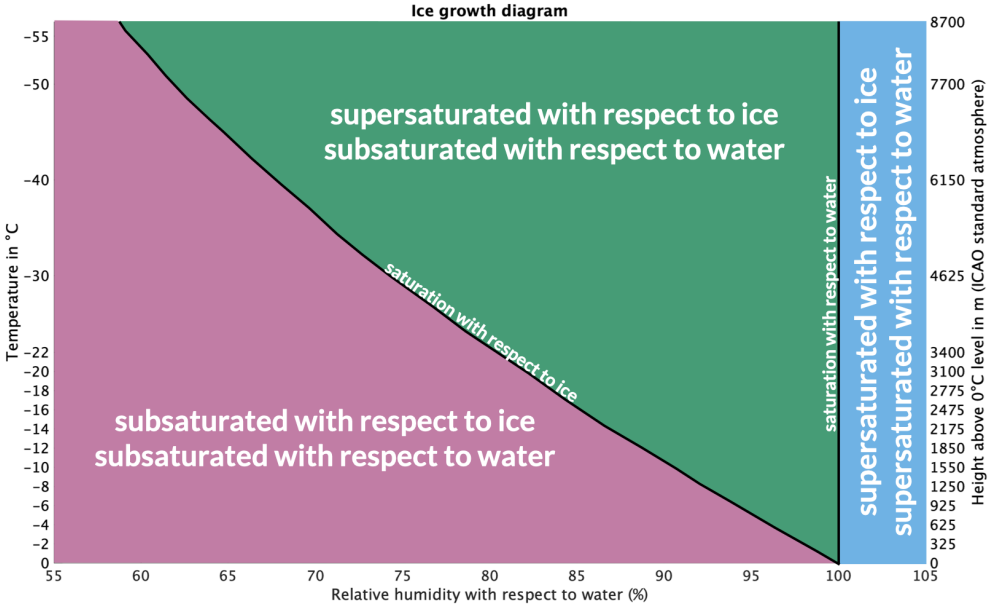

FIG. 4: Simplified diagram illustrates the phase space of subsaturated and supersaturated conditions with respect to water and ice in terms of RH_w and air temperature.

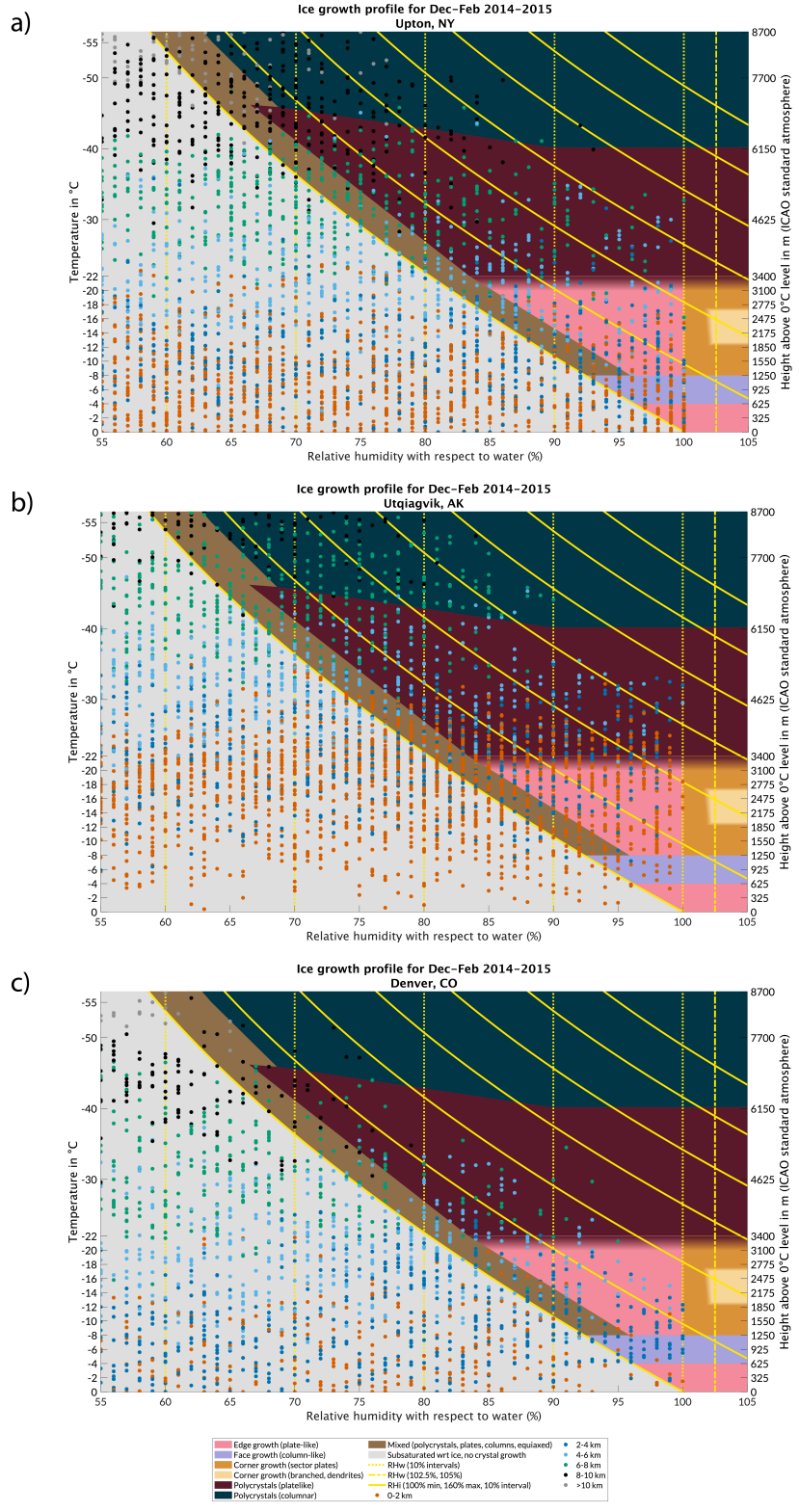

FIG. 5: Seasonal sounding profiles for three locations during the winter of December 2014 - February 2015 overlaid on the ice growth diagram. a) From the NWS radiosonde site at Upton, NY (178 profiles). b) From the DOE radiosonde site at Utqiagvik, AK (180 profiles). c) From the NWS radiosonde site at Denver, CO (179 profiles). Dot colors represent altitude of measurements in 2 km intervals. See key for details.

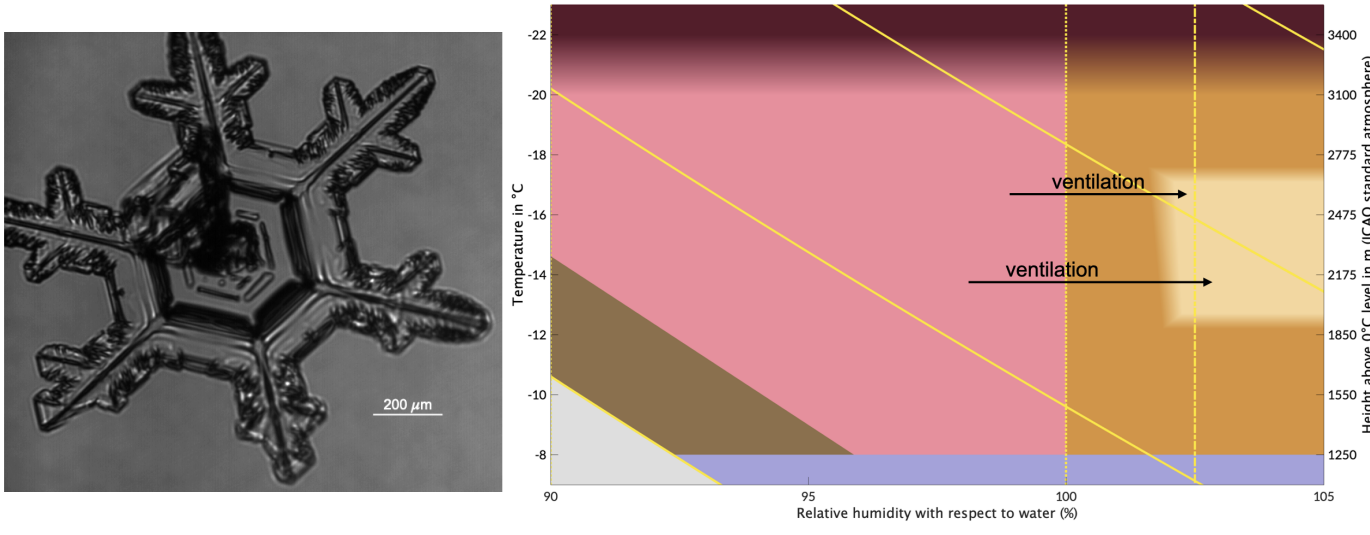

FIG. 6: CPI image at 22:08:38 UTC on January 25, 2020 at 4.86 km altitude of crystal formed by a sequence of edge growth to corner growth, with possible physical pathways annotated on the ice growth diagram. (Kikuchi et al. (2013) classification: plate with branches, P4e).

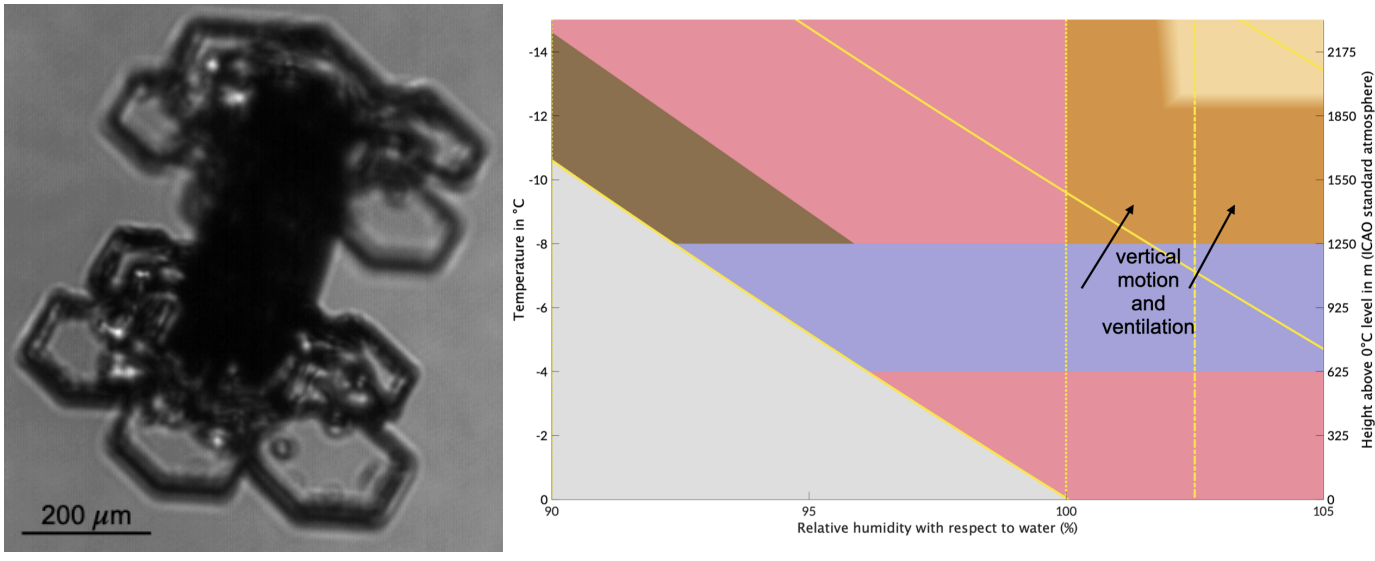

FIG. 7: CPI image at 22:05:45 UTC on January 25, 2020 at 4.21 km altitude of crystal formed by a sequence of face growth to corner sector growth, with possible physical pathways annotated on the ice growth diagram. (Kikuchi et al. (2013) classification: column with dendrites, CP1b).

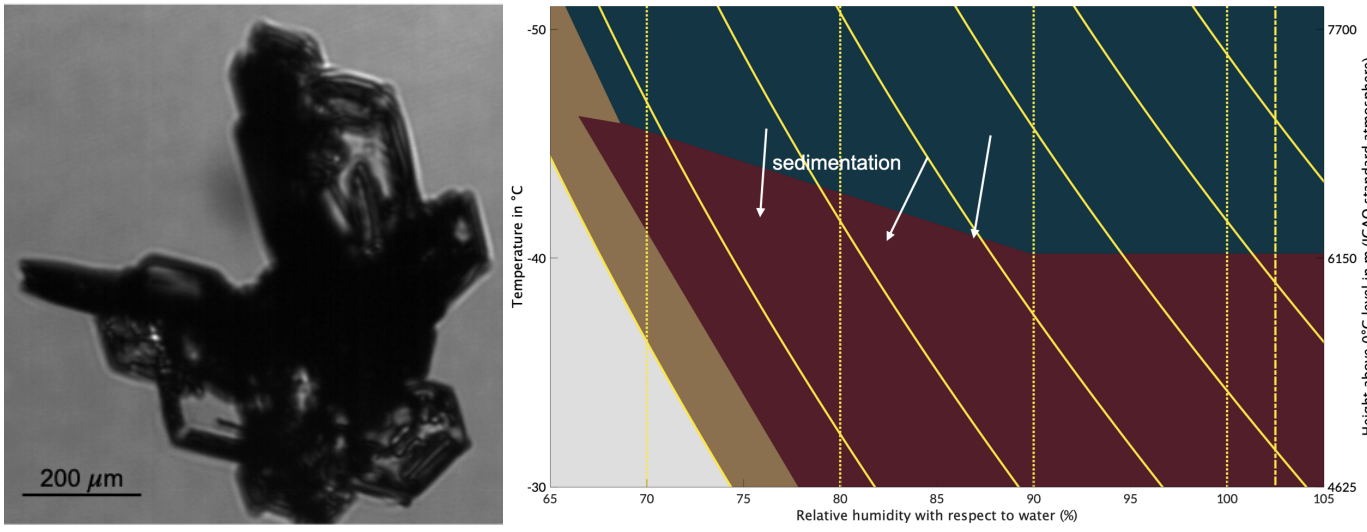

FIG. 8: CPI image at 22:08:52 UTC on January 25, 2020 at 4.86 km altitude of crystal formed by a sequence of polycrystal (columnar) to polycrystal (platelike) growth, with possible physical pathways annotated on the ice growth diagram. (Kikuchi et al. (2013) classification: radiating assemblage of plates, P7a).

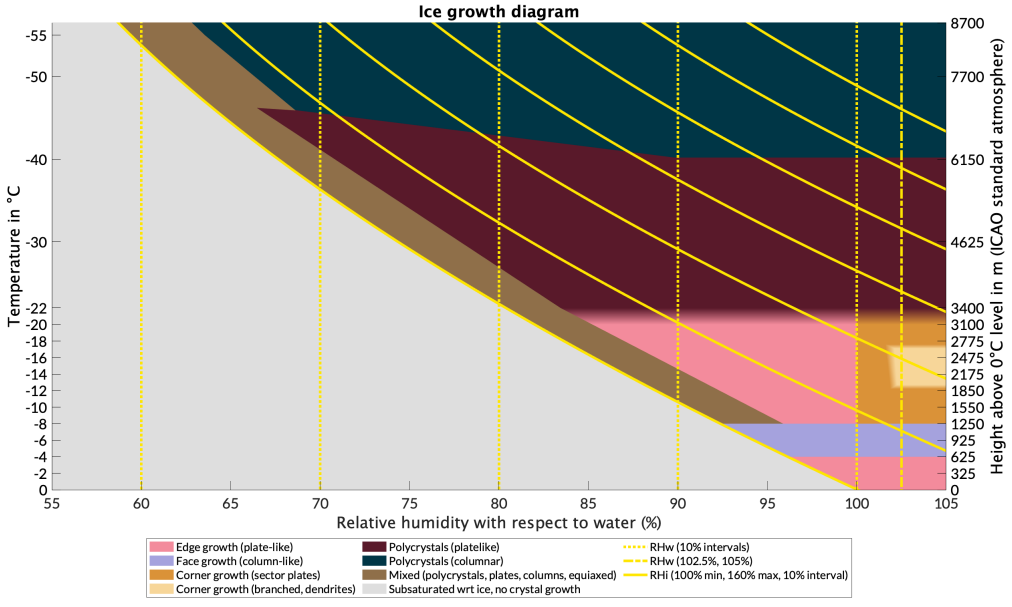

Fig. A1: The applied ice growth diagram in terms of relative humidity with respect to water. This version is designed to have a high-contrast color scheme, appropriate for use as a base layer for data visualization.

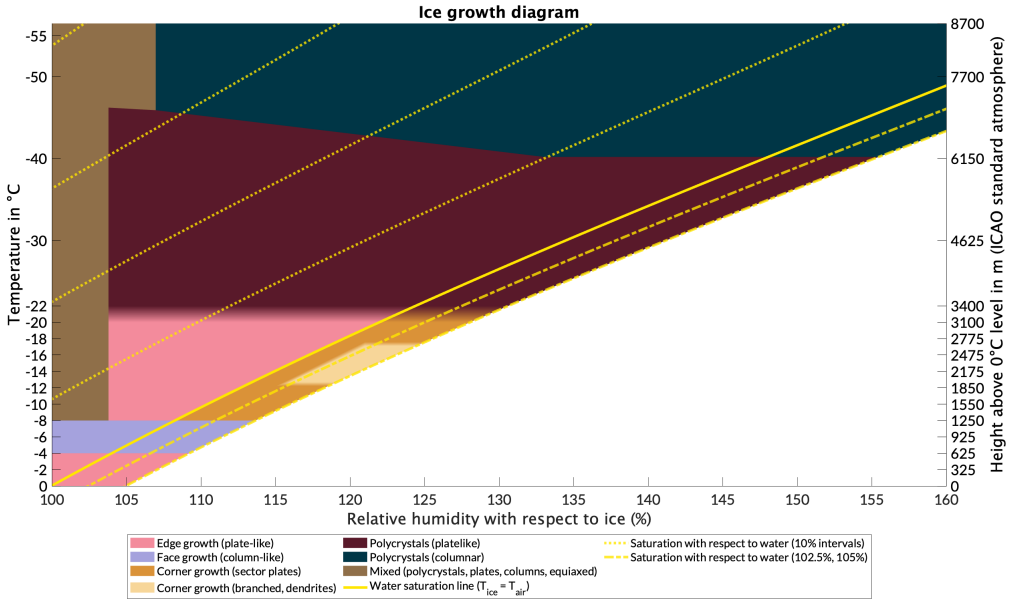

Fig. A2: The applied ice growth diagram in terms of relative humidity with respect to ice. This version is designed to have a high-contrast color scheme, appropriate for use as a base layer for data visualization.

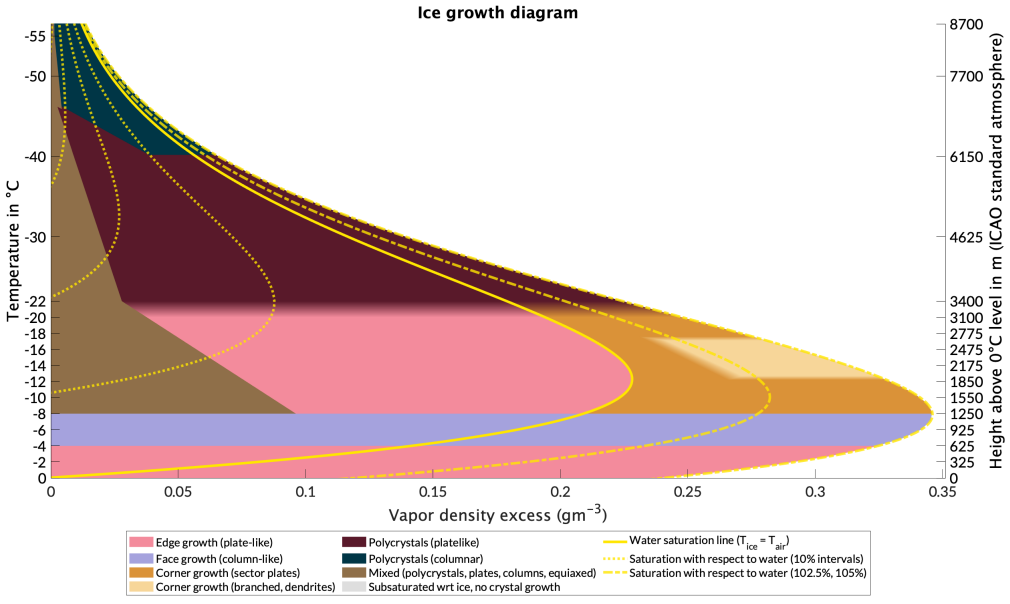

Fig. A3: The applied ice growth diagram in terms of vapor density excess. This version is designed to have a high-contrast color scheme, appropriate for use as a base layer for data visualization.